A Parameter Optimization Approach for the Optimal Control of Large-Scale Musculoskeletal Systems

M. G. Pandy

F. C. Anderson
Department of Kinesiology and Health Education.

D. G. Hull
Department of Aerospace Engineering and Engineering Mechanics.

University of Texas at Austin, Austin, Texas 78712

This paper describes a computational method for solving optimal control problems involving large-scale, nonlinear, dynamical systems. Central to the approach is the idea that any optimal control problem can be converted into a standard nonlinear programming problem by parameterizing each control history using a set of nodal points, which then become the variables in the resulting parameter optimization problem. A key feature of the method is that it dispenses with the need to solve the two-point, boundary-value problem derived from the necessary conditions of optimal control theory. Gradient-based methods for solving such problems do not always converge due to computational errors introduced by the highly nonlinear characteristics of the costate variables. Instead, by converting the optimal control problem into a parameter optimization problem, any number of well-developed and proven nonlinear programming algorithms can be used to compute the near-optimal control trajectories. The utility of the parameter optimization approach for solving general optimal control problems for human movement is demonstrated by applying it to a detailed optimal control model for maximum-height human jumping. The validity of the near-optimal control solution is established by comparing it to a solution of the two-point, boundary-value problem derived on the basis of a bang-bang optimal control algorithm. Quantitative comparisons between model and experiment further show that the parameter optimization solution reproduces the major features of a maximum-height, countermovement jump (i.e., trajectories of body-segmental displacements, vertical and fore-aft ground reaction forces, displacement, velocity, and acceleration of the whole-body center of mass, pattern of lower-extremity muscular activity, jump height, and total ground contact time).

Introduction

In recent years, there have been a number of attempts to apply optimal control theory to the analysis of human movement [1–5]. All of these attempts have been motivated by the belief that optimal control theory is a useful tool for elucidating the control of the human musculoskeletal system.

A classic example is the quantification of individual, time-varying muscle forces. Muscle forces not only play a major role in determining the stresses in bones and joints, but they also reflect the underlying neural control processes responsible for the observed movement patterns. Unfortunately, invasive techniques for measuring muscle forces are highly objectionable, whereas noninvasive techniques such as electromyography (EMG) do not provide the quantitative accuracy needed to define muscle's action on the skeleton. In addition, the human musculoskeletal system is mechanically redundant (i.e., the number of muscles spanning a joint exceeds the number of degrees of freedom defining joint motion) so that a direct solution of the muscle force-joint torque equations is not possible. To circumvent this difficulty, previous investigators have used both static optimization [6, 7] and optimal control techniques [2, 4, 5] to estimate muscle forces during movement.

A major advantage of using optimal control theory is that it allows both muscle excitation-contraction and musculotendon dynamics to be taken into account. Unfortunately, optimal control problems involving musculoskeletal systems are difficult to solve because they are characterized by nonlinear skeletal and musculotendon dynamics, high dimensionality (i.e., there are many states), unusual path constraints, and controls (i.e., muscle excitations) that are neither bang-bang nor linear. In fact, complete analytical solutions to such problems are not possible, whereas computational algorithms for deriving the optimal controls are difficult to develop and implement.

The classical approach for computing the optimal controls of a dynamical system involves the use of variational techniques

Contributed by the Bioengineering Division for publication in the JOURNAL OF BIOMECHANICAL ENGINEERING. Manuscript received by the Bioengineering Division April 2, 1991; revised manuscript received April 6, 1992. Associate Technical Editor: B. R. Simon.

[8]. In general, the variational approach produces a set of necessary conditions which result in a nonlinear, two-point, boundary-value problem (TPBVP) that cannot be solved analytically since the boundary conditions on the state-costate equations are split (i.e., only the initial conditions for the state equations and the terminal conditions for the costate equations are known). Instead, computational solutions of the TPBVP are obtained by forward integrating the state equations and backward integrating the costate equations [9]. This approach, though straightforward, is not robust due to the highly nonlinear characteristics of the costate variables.

An alternative to solving the TPBVP involves converting the optimal control problem into an algebraic *parameter optimization* problem [10–14]. Recently, Nagurka and Yen [11] used an inverse-dynamics approach to approximate the time response of each generalized coordinate by the sum of a polynomial in time and a finite number of terms defining a Fourier-type series. In this way, the optimal control problem was converted into a parameter optimization problem, in which the coefficients of the Fourier functions, the free boundary conditions, and the terminal time were the variables optimized. An important advantage of the inverse-dynamics formulation is that it does not require the system differential equations to be numerically integrated. Instead, the parameter optimization solution comprises a set of near-optimal state trajectories, from which the input control histories are computed. A major disadvantage of this method, however, is that it cannot cope with optimal control problems that are bang-bang [11].

In contrast to the inverse-dynamics method, the direct-dynamics technique described by Goh and Teo [12] is based upon the idea that any control history can be parameterized using a set of *nodal points*, from which the control function is reconstructed by simple linear interpolation. In this way, the optimal control problem is recast as a parameter optimization problem, in which the system differential equations are integrated forwards in time and the nodal points are the variables optimized. The major advantage of, and indeed the primary motivation for, converting the optimal control problem into a parameter optimization problem is that it circumvents the computational hazards surrounding a solution of the TPBVP. Instead, any number of well-developed and proven nonlinear programming algorithms (e.g., [15]) can be used to solve the resulting parameter optimization problem. As we shall demonstrate, the parameter optimization approach is especially attractive when dealing with large-scale, nonlinear, dynamical systems, as exemplified by a detailed mathematical model of the human musculoskeletal system.

Parameter Optimization Approach

Optimal Control Problem. In general, any nonlinear, dynamical system can be represented by

$$\dot{\mathbf{x}} = \mathbf{f}(\mathbf{x}, \mathbf{u}, t) \tag{1}$$

where $\mathbf{x}$ is an $n \times 1$ vector of state variables, $\mathbf{u}$ is an $m \times 1$ vector of control variables, $\mathbf{f}$ is an $n \times 1$ vector function, and t is time. The object of the control $\mathbf{u}$ is to operate the system between a specified initial state

$$\mathbf{x}(0) = \mathbf{x}_0 \tag{2}$$

and a constrained final state

$$\psi(t_f, \mathbf{x}_f) = \mathbf{0} \tag{3}$$

where ψ is a $p \times 1$ vector function, and $\mathbf{x}_f$ is the state evaluated at the final time, t_f. (For the more general case in which some of the initial states are free, the parameter optimization approach remains applicable, though the formulation presented below must be modified.)

In addition to the boundary conditions, Eqs. (2)–(3), the controls $\mathbf{u}$ and the states $\mathbf{x}$ may be bounded by inequality constraints

$$\mathbf{C}(\mathbf{x}, \mathbf{u}, t) \le \mathbf{0} \tag{4}$$

and

$$\mathbf{S}(\mathbf{x}, t) \le \mathbf{0}, \tag{5}$$

where $\mathbf{C}$ and $\mathbf{S}$ are $q \times 1$ and $r \times 1$ vector functions, respectively.

Though there are an infinite number of control histories $\mathbf{u}$ which can perform the above task, a particular set will deliver the "best" response; and this choice is dictated by the performance criterion (e.g., minimum time). In general, the performance index is given by

$$J = \phi(t_f, \mathbf{x}_f) + \int_0^{t_f} L(\mathbf{x}, \mathbf{u}, t)dt \tag{6}$$

where ϕ and L are scalar functions of the indicated arguments.

Therefore, the optimal control problem is to determine the control histories $\mathbf{u}$ which minimize the performance criterion (Eq. (6)) subject to the system differential equations (Eq. (1)), the prescribed boundary conditions (Eqs. (2)–(3)), the control-variable inequality constraints (Eq. (4)), and the state-variable inequality constraints (Eq. (5)).

Parameter Optimization Problem. The optimal control problem (Eqs. (1)–(6)) is converted into a parameter optimization problem in *three* steps. First, the performance index (Eq. (6)) and the control- and state-variable inequality constraints (Eqs. (4)–(5)) must be converted to point conditions. The performance index can be converted to a point condition by introducing the differential equation

$$\dot{x}_{n+1} = L \tag{7}$$

and boundary condition

$$x_{n+1}(0) = 0, \tag{8}$$

where x_{n+1} is the $(n+1)$th state. Thus, Eq. (6) becomes

$$J = \phi(t_f, \mathbf{x}_f) + x_{n+1}(t_f), \tag{9}$$

where

$$x_{n+1}(t_f) = \int_0^{t_f} L(\mathbf{x}, \mathbf{u}, t)dt. \tag{10}$$

Similarly, each control- and state-variable inequality constraint can be converted to a point condition by forming an integral over the region the constraint is violated and forcing the value of the integral to zero. For example, if

$$S_i(\mathbf{x}, t) \le 0, \tag{11}$$

where $S_i(\mathbf{x}, t)$ is the ith scalar function, an appropriate integral inequality constraint would be

$$\int_0^{t_f} \min^2(-S_i(\mathbf{x}, t), 0)dt \le 0, \tag{12}$$

where $\min(-S_i(\mathbf{x}, t), 0)$ indicates the minimum value of the quantities in the parentheses. The integral constraint, Eq. (12), can be converted into a differential equation

$$\dot{x}_{n+i} = \min^2(-S_i(\mathbf{x}, t), 0) \tag{13}$$

and boundary condition

$$x_{n+i}(0) = 0, \tag{14}$$

where x_{n+i} is the $(n+i)$th state. Thus, the state-variable inequality constraint, Eq. (11), is replaced by

$$x_{n+i}(t_f) \le 0. \tag{15}$$

In this way, all of the $q + r$ control- and state-variable inequality constraints (Eqs. (4) and (5)) can be converted into differential equations and algebraic constraints (Eqs. (13)–(15)).

If the resulting $q + r$ states, together with the state contributed by the performance index (Eq. (7)), are adjoined to

the original $n \times 1$ state vector $\mathbf{x}$, the optimal control problem (Eqs. (1)–(6)) can be restated as: Determine the control histories $\mathbf{u}$ which minimize the performance criterion

$$J = \Phi(t_f, \mathbf{y}_f) \tag{16}$$

subject to the system differential equations

$$\dot{\mathbf{y}} = \mathbf{F}(\mathbf{y}, \mathbf{u}, t), \tag{17}$$

the prescribed boundary conditions

$$\mathbf{y}(0) = \mathbf{y}_0, \tag{18}$$

the p equality constraints

$$\Psi(t_f, \mathbf{y}_f) = \mathbf{0}, \tag{19}$$

and the $q + r$ inequality constraints

$$\Theta(t_f, \mathbf{y}_f) \leq \mathbf{0}. \tag{20}$$

Here $\mathbf{y}$ is the transformed $n + q + r + 1$ state vector comprising the original state variables $\mathbf{x}$ as well as the states derived from converting the performance index and the control- and state-variable inequality constraints to point conditions.

The second step in the conversion of the optimal control problem involves making the final time (t_f) a parameter. This is done by normalizing time:

$$\tau = t/t_f, \tag{21}$$

which fixes the interval of integration so that the system differential equations (Eq. (17)) become

$$\mathbf{y}' = t_f \mathbf{F}(\mathbf{y}, \mathbf{u}, \tau); \quad 0 \leq \tau \leq 1; \quad \mathbf{y}' = \frac{d\mathbf{y}}{d\tau}. \tag{22}$$

In the third and final step, the control histories $\mathbf{u}$ are parameterized by introducing a prespecified number of *nodal points*, from which trajectories of the controls can be reconstructed using linear interpolation. If w nodal points are chosen for each of the m control histories $\mathbf{u}$, the kth control history $u_k(\tau)$ is

$$u_k(\tau) = u_k(\mathbf{a}_k, \tau), \tag{23}$$

where $\mathbf{a}_k$ is a $w \times 1$ vector of control nodal points. Thus, a single vector $\mathbf{z}$ can be used to represent the $(m \times w) + 1$ parameters specifying the control nodal points and the final time, t_f:

$$\mathbf{z}^T = [\mathbf{a}_1^T, \mathbf{a}_2^T, \ldots, \mathbf{a}_m^T, t_f]. \tag{24}$$

If values are assigned to these variables (i.e., if an initial guess is provided for the control nodal points and the final time), Eq. (22) can be integrated forwards in time (using the boundary condition defined by Eq. (18)) to compute the values of the states at the final time, that is:

$$\mathbf{y}_f = \mathbf{G}(\mathbf{z}). \tag{25}$$

Therefore, it is apparent that the state vector $\mathbf{y}_f$ can be eliminated from the optimal control problem to give the following parameter optimization problem: Find the parameters $\mathbf{z}$ which minimize the performance criterion

$$J = Q(\mathbf{z}) \tag{26}$$

subject to the p equality constraints

$$C_i(\mathbf{z}) = 0; \quad i = 1, p \tag{27}$$

and the $q + r$ inequality constraints

$$C_j(\mathbf{z}) \leq 0; \quad j = 1, (q + r). \tag{28}$$

Parameter Optimization Algorithm. To solve the above parameter optimization problem, we devised the computational algorithm given in Fig. 1. With arbitrary initial guesses for the parameters each iteration begins with a forward integration of the system differential equations (Eq. (22)) to compute the values of the performance index (Eq. (26)) and the constraints (Eqs. (27)–(28)) (Fig. 1, Step 3). First derivatives of each of these quantities with respect to the variables $\mathbf{z}$ are then calculated using forward differences (Fig. 1, Step 4). Finally, values of the performance index, the constraints, and their derivatives are input into a nonlinear programming algorithm, based upon sequential quadratic programming [15],

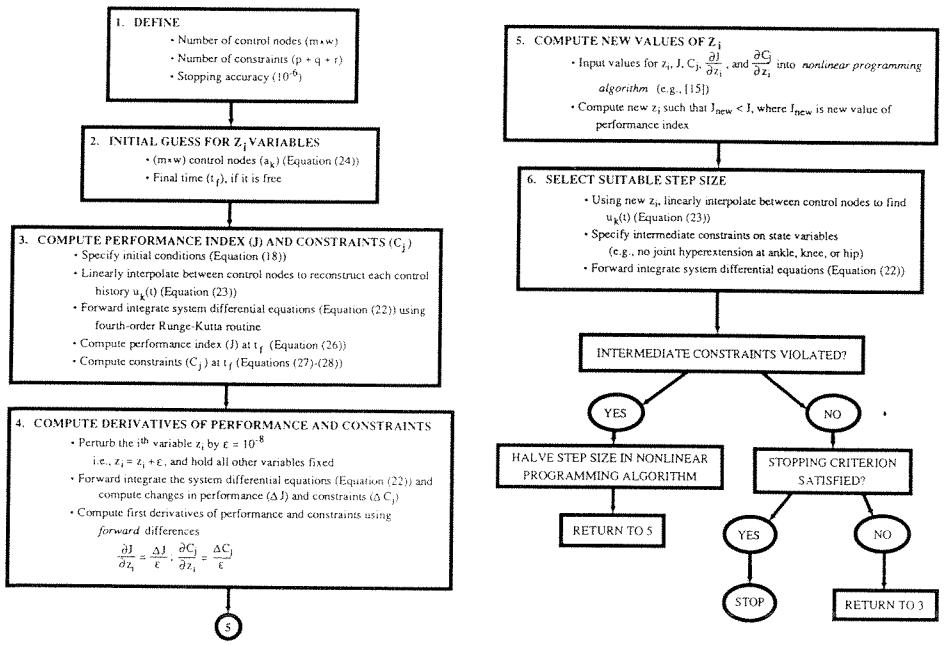

Fig. 1 Flowchart showing the order in which iterative computations are performed in the parameter optimization algorithm. A single iteration of the algorithm comprises Steps 3 and 6. Note that, for optimal control problems for human movement, the step size at each iteration is selected by specifying appropriate intermediate constraints on the state variables (e.g., no hyperextension of the lower-extremity joints during the ground contact phase of jumping; Step 6). Equations referred to are given in the text.

to obtain improved estimates of the variables **z** (i.e., the controls **u** and final time t_f) (Fig. 1, Step 5).

As with any other optimal control or nonlinear programming algorithm, a key feature of our parameter optimization algorithm is the selection of a step size at each iteration (Fig. 1, Step 6). If too large a step is taken in the direction of the calculated search direction, the controls can be altered in a disastrous fashion. Specifically, large step sizes can produce radically different, and therefore spurious, state trajectories. To circumvent this difficulty, changes in the controls were made by computing a step size based upon an appropriate set of intermediate path constraints (e.g., no joint hyperextension during the ground contact phase of a maximum-height jump; see Results). To illustrate the performance of our parameter optimization algorithm, we have included the solution to a standard optimal control problem in the Appendix.

Application to Jumping

We now demonstrate the utility of the parameter optimization approach by applying it to determine the optimal controls (i.e., muscle excitations) for maximum-height human jumping. In particular, we present a detailed optimal control solution to a two-legged, countermovement jump (CMJ). Though the details of our musculoskeletal model and optimal control problem for vertical jumping are given elsewhere [5], for completeness, we summarize each of these below.

Human Experiments. Five strong, athletic, adult males (age 27 ± 7 yr, height 183 ± 3 cm, and body mass 78 ± 5 kg) were chosen as subjects for these experiments. From a relaxed, standing position, and with hands on shoulders, each subject performed a two-legged CMJ (i.e., a vertical jump involving significant downward motion of the center of mass of the body prior to upward propulsion) under the command "jump as high as possible." For five consecutive jumps, force-plate, limb motion, and EMA data were recorded simultaneously.

Ground reaction forces were measured using a BERTEC six-component, strain-gaged force platform, having a first natural frequency of 1500 Hz (vertical channel). Fore-aft and vertical channels were sampled at 1000 Hz, as were analog EMG data. Pairs of EMG-preamplifier surface electrodes (center-to-center distance 4 cm; circumference 12 mm) were attached to the right lower-extremity of each subject to record activity in seven muscle groups: soleus (SOL), gastrocnemius (GAS), tibialis anterior (TA), vasti (VAS), rectus femoris (RF), hamstrings (HAMS), and gluteus maximus (GMAX) (Fig. 2).

To record the limb-segmental angular displacements of each subject, retroreflective markers were positioned over six bony prominences: head of the fifth metatarsophalangeal joint, calcaneus, lateral malleolus, lateral epicondyle, greater trochanter, and glenohumeral joint. Together, these landmarks defined four body segments: the foot, shank, thigh, and HAT segment (head, arms, and trunk). With a video-based, kinematic, data-acquisition system (Motion Analysis Inc., Santa Rosa, CA), absolute displacements were recorded at 60 Hz (i.e., displacements of each landmark were referenced to an inertial frame fixed on the force platform). All post-processing of these data was carried out on a SUN Sparc 1-plus, color-graphics, computer workstation.

Musculoskeletal Model. We modeled the human body as a four-segment, articulated, planar linkage, with adjacent links joined together by frictionless revolutes. A total of eight lower-extremity musculotendinous units provided the actuation in the model (Fig. 2). Each musculotendinous unit was modeled as a three-element, lumped-parameter entity, muscle, in series with tendon. The mechanical behavior of muscle was described by a Hill-type contractile element which modeled its force-length-velocity-activation property, a series-elastic element which modeled its short-range stiffness, and a parallel-elastic element which modeled its passive response. The elastic properties of tendon were modeled by a linear stress-strain (σ-ϵ) curve. The details of our musculotendon model are given in [5].

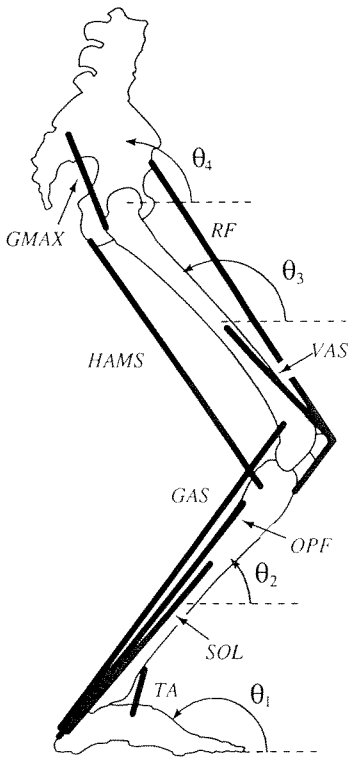

Fig. 2 Schematic representation of the musculoskeletal model for the vertical jump. Symbols appearing in the diagram are: soleus (SOL), gastrocnemius (GAS), other plantarflexors (OPF), tibialis anterior (TA), vasti (VAS), rectus femoris (RF), hamstrings (HAMS), and gluteus maximus (GMAX). θ_1, θ_2, θ_3, θ_4 are segmental angles of the foot, shank, thigh, and HAT (head, arms, and trunk), respectively.

Musculotendinoskeletal Dynamics. The dynamical equations for the overall musculotendinoskeletal system are

$$\ddot{\theta} = A(\theta)^{-1}[B(\theta)\dot{\theta}^2 + C(\theta) + DM(\theta)\mathbf{P}^T + T(\theta, \dot{\theta})] \quad (29)$$

$$\dot{\mathbf{P}}^T = f_i(\theta, \dot{\theta}, P_i^T, a_i);\ i = 1, 8 \quad (30)$$

$$\dot{\mathbf{a}} = (1/\tau_{\text{rise}})(1 - a_i)u_i + (1/\tau_{\text{fall}})(a_{\min} - a_i)(1 - u_i);\ i = 1,8 \quad (31)$$

where θ, $\dot{\theta}$, $\ddot{\theta}$ are vectors of limb angular displacement, velocity, and acceleration (all are 4 × 1) (Fig. 2); $T(\theta, \dot{\theta})$ is a 4 × 1 vector of externally applied joint torques containing the moment applied to the foot segment from a highly-stiff, damped, torsional spring; $\mathbf{P}^T$ is a 8 × 1 vector of musculotendon actuator forces; $M(\theta)$ is a 3 × 8 moment-arm matrix formed by computing the perpendicular distance between each musculotendon actuator and the joint it spans; $A(\theta)$ is the 4 × 4 system mass matrix; $C(\theta)$ is a 4 × 1 vector containing only gravitational terms; $B(\theta)\dot{\theta}^2$ is a 4 × 1 vector describing both Coriolis and centrifugal effects, where $\dot{\theta}^2$ represents $\dot{\theta}_j^2$ for $i = 1, 4$; D is a 4 × 3 matrix which transforms joint torques into segmental torques; $a(t)$ is muscle activation; $u(t)$ is the net neural control signal to the muscle (i.e., we do not dissociate the "net" firing rate control of a muscle from the recruitment control [16]); τ_{rise} and τ_{fall} are rise and decay time constants for muscle activation respectively; and $a_{\min}$ is a designated lower bound on muscle activation introduced to cope with problems associated with inverting the force-velocity curve of muscle at low activation levels [17]. In our model, the state vector **x** is composed of 24 elements: four angular displacements θ_i, $i = 1, 4$, four angular velocities $\dot{\theta}_i$, $i = 1, 4$, eight

muscle activations a_i, $i = 1, 8$, and eight musculotendon actuator forces P_i^T, $i = 1, 8$. The details of Eqs. (29)–(31) appear in [5].

Of particular importance to this paper is our model for muscle excitation-contraction dynamics. Equation (31) was constructed under the assumption that the optimal controls for maximum-height jumping are bang-bang (i.e., $u(t) = 0$ or 1). Therefore, it does not accurately model muscle activation at intermediate values of $u(t)$ (see [5] for details). To rectify this, we have constructed a first-order differential equation for muscle excitation-contraction dynamics that is *nonlinear* in the control $u(t)$:

$$\frac{da(t)}{dt} = (1/\tau_{\text{rise}})(u - a)u + (1/\tau_{\text{fall}})[u - (a - a_{\min}) - (u - a)u] \quad (32)$$

Equation (32) now models muscle activation ($a(t)$) at any value of $u(t)$ between 0 and 1. At steady state, this relationship causes muscle activation ($a(t)$) to follow the input neural excitation ($u(t)$). Note that the rise and decay time constants for muscle activation are the same in Eqs. (31) and (32) (i.e., $\tau_{\text{rise}} = 20$ ms and $\tau_{\text{fall}} = 200$ ms [16]).

Musculotendon Properties, Musculoskeletal Geometry, and Scaling. Parameters defining nominal muscle properties (i.e., peak isometric force and the corresponding pennation angle and length of the muscle fiber) for each of the eight musculotendinous units in the model were estimated from data reported by Wickiewicz et al. [18] and Brand et al. [19]. The linear σ-ϵ curve for tendon was specified using values of elastic moduli obtained from Alexander and Vernon [20], Woo et al. [21], and Butler et al. [22], while cross-sectional areas were obtained from anatomy textbooks if tendon had a well defined component external to the muscle. Otherwise, tendon cross-sectional area was chosen to give a reasonable strain at peak isometric force (i.e., in the range 2–6 percent). Parameters defining muscle and tendon properties used in the model are given in Table 1 of [5]. Body-segmental parameters for the model (i.e., segment mass and length, moment of inertia, and location of the center of mass of each segment) were scaled according to subject height and weight using nominal data reported by Winter [23] (see Appendix 1 in [5]).

The musculoskeletal geometry of the model (musculotendon origin and insertion sites) was defined on the basis of data reported by Brand et al. [24]. Rather than give the effective origin and insertion sites, we instead show plots of maximum isometric torque versus joint angle for the ankle, knee, and hip (Fig. 3, heavy solid lines). Also given in Fig. 3 are the corresponding experimental torque-angle data reported in the literature (e.g., [25]). The agreement between model and experiment (compare heavy solid lines with data points in Fig. 3) is reasonable for all of the lower-extremity joints, with the experimental data in some cases being offset by as much as twenty degrees from the torque generated by the model (e.g., Fig. 3(*c*) hip, compare solid line with data points at 160 degrees). Such differences, however, may be due to experimental error (e.g., errors in the measurement of joint angle and torque), rather than inaccuracies in the musculotendon properties and musculoskeletal geometry assumed by our model.

To estimate body strength-to weight ratio, we instructed each subject to perform a series of maximal, voluntary, isometric contractions. Using a Biodex dynamometer, we measured the active, extensor moment exerted about the knee at various joint angles. We then computed body strength-to-weight ratio by dividing peak isometric knee torque by overall body weight. The strength-to-weight ratio of the model was *scaled* to that of our subjects by uniformly adjusting the peak isometric force of all the extensor muscles spanning the knee until the isometric, extensor knee torque in the model matched that generated by our subjects (Fig. 4, compare empty square with filled circle and heavy solid line). Finally, we used the average increase in peak knee torque generated by our subjects, over the nominal values reported in the literature (Fig. 4, difference between empty square and filled circle), to uniformly adjust the peak isometric strength of all the extensor muscles spanning the ankle and hip in the model, assuming that muscle strength increases uniformly throughout the lower-extremity [26].

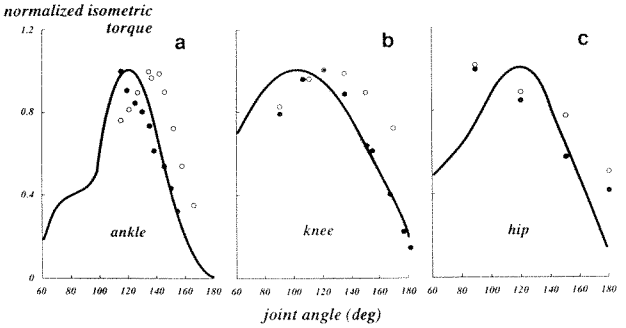

Fig. 3 Normalized isometric torque-angle curves of the musculoskeletal model. Heavy solid line is the sum of all the extensor torques at the ankle (*a*), knee (*b*), and hip (*c*). Note that the shaded bars represent the range of angles covered during a maximum-height CMJ. Also, note that hip angle = 180 + θ_3 − θ_4; knee angle = 180 − θ_2 + θ_3; and ankle angle = 180 − θ_1 + θ_2, where θ_1, θ_2, θ_3, θ_4 are segmental angles defined in Fig. 2. In each case, muscle is assumed to be fully activated, and the torques generated are those only due to active muscle. For all muscles, tendon slack lengths were adjusted until realistic torque-angle curves were obtained (see [40] for details). Each curve has been normalized by the peak torque at each joint generated by all the muscles. These values were 390, 300, and 330 Nm for the ankle, knee, and hip, respectively. Similarly, experimental data were normalized by their respective peak values of torque. The experimental data were obtained from:

(*a*) ankle: ○ [41]; • [42].

(*b*) knee: ○ [25]; • [43].

(*c*) hip: ○ [44]; • [45].

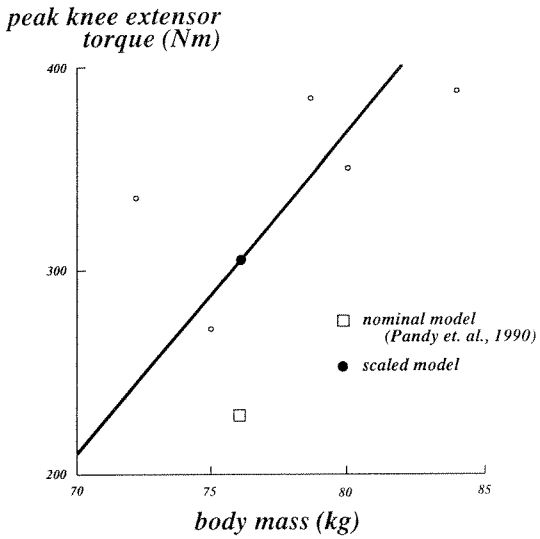

Fig. 4 Peak knee extensor torque generated by the model (filled circle) and our subjects (empty circles) during a maximal, voluntary, isometric contraction versus total body mass. All experimental joint torques were measured on a Biodex dynamometer. For all subjects, peak, isometric, knee extensor torque occurred at approximately 100 degrees of knee flexion. The empty square represents the peak isometric knee extensor torque generated by the model using the nominal musculotendon properties reported in Table 1 of [5].

Optimal Control Problem. Given that maximum-height jumping presents a relatively unambiguous performance cri-

terion, it fits well into the framework of optimal control theory. We chose the height reached by the center of mass of the body to be the measure of performance:

$$J(\theta, \dot{\theta}, t_f) = Y_c(t_f) + \dot{Y}_c^2(t_f)/2g \tag{33}$$

where $Y_c(t_f)$ and $\dot{Y}_c(t_f)$ are the vertical position and velocity of the center of mass of the body at time t_f, the instant at which lift-off occurs, and g is the gravitational acceleration constant.

The constraints which define the problem are the system differential equations (Eqs. (29)–(31)), a set of inequality constraints which bound the magnitude of each muscle excitation signal:

$$0 \le u_i \le 1; \quad i = 1, 8 \tag{34}$$

and a terminal equality constraint that specifies the instant the body leaves the ground (i.e., a zero vertical ground reaction force at the final time t_f):

$$F_v(\theta, \dot{\theta}, \ddot{\theta})|_{t_f} = \sum_{i=1}^{4} m_i(\ddot{Y}_{c_i} + g)|_{t_f} = 0, \tag{35}$$

where m_i is the mass of the ith segment, $\ddot{Y}_{c_i}$ is the vertical acceleration of the center of mass of the ith segment, $F_v(\theta, \dot{\theta}, \ddot{\theta})$ is the magnitude of the vertical ground reaction force, and $|_{t_f}$ indicates that each quantity is evaluated at the final time.

Thus, the optimal control problem is to maximize jump height (Eq. (33)), subject to the given initial conditions $\mathbf{x}(0) = \mathbf{x}_0$, the system differential equations (Eqs. (29)–(31)), a set of control-variable inequality constraints (Eq. (34)), and a state-variable, terminal-equality constraint (Eq. (35)). Note that the optimal control problem as formulated here is a free-final-time problem.

With the model in a static, standing position (i.e., prespecified segmental angular displacements and zero angular velocities), we chose the initial activations of all the uniarticular muscles to be as low as possible (i.e., $a_i(0) = 0.05$, $i = 1, 5$, since each subject began the jump from an upright, relaxed posture), and then computed the corresponding muscle forces using Eq. (30) with $\mathbf{P}^T = 0$ (i.e., under static conditions). The initial muscle forces (and activations) for all the biarticular actuators were then found by constraining the model to be in static equilibrium (i.e., zero angular acceleration of all the body segments at time $t = 0$).

Computation of the Optimal Controls. Previously, Pandy et al. [5] hypothesized that the optimal controls for maximum-height jumping are bang-bang (i.e., the muscle excitations can be only zero or one). Accordingly, Eq. (31) was constructed to model muscle excitation-contraction dynamics, in which case the system Hamiltonian is linearly dependent upon the controls, and the optimal controls must be bang-bang. With Eq. (31) modeling muscle excitation-contraction dynamics, we computed the bang-bang optimal controls for a maximum-height CMJ using a modified version of an algorithm developed by Polak and Mayne [27]. Briefly, at each iteration, the TPBVP was solved by forward integrating the state equations, using an arbitrary initial guess for the controls. The forward integration proceeded until the terminal equality constraint (Eq. (35)) was met (i.e., the vertical ground reaction force became zero), at which point the costate equations were integrated backwards in time using a boundary condition on the costates computed from the state at lift-off. The costates corresponding to muscle activation were then used to find a new set of control switching times that increased jump height (see [28] for details).

To relax the assumption of bang-bang optimal controls for jumping, we constructed Eq. (32) to model muscle excitation-contraction dynamics. In this case, because the system Hamiltonian is nonlinearly dependent upon the controls, the optimal control problem is *not* bang-bang (i.e., the muscle excitations $u(t)$ can take values anywhere between 0 and 1). Thus, the modified Polak-Mayne optimal control algorithm [28] cannot be applied. Instead, we converted the optimal control problem into a parameter optimization problem by normalizing time (Eq. (21)) and parameterizing each control history using 21 control nodes, each spaced 0.05 t_f s apart. Our choice of 21 control nodes for each muscle was based purely upon computational experience. We found that the parameter optimization solution becomes too sensitive to even small changes in the controls when fewer than 21 control nodes are used (see also Appendix), whereas a larger number of control nodes increases computational time without significantly improving the accuracy of the near-optimal control solution. (In general, the number of control nodes should be increased until there is little or no change in the predicted optimal control solution.) Thus, a total of 169 variables were optimized for jumping (i.e., 21 control nodes for each of the eight lower-extremity muscles, in addition to the final time, t_f). We solved this parameter optimization problem using the algorithm given in Fig. 1.

Results

Comparison of Model and Experiment. In general, there is good agreement between model and experiment. Jump height for our five subjects ranged from 49 cm to 60 cm, while corresponding values for the model predicted by the optimal control and parameter optimization solutions were 61 cm and 64 cm, respectively. Final lift-off times for the model and subjects were also in reasonable agreement, with values for the optimal control and parameter optimization solutions being 0.87 s and 1.03 s, respectively, compared to lift-off times for our subjects ranging from 1.1 s to 1.3 s.

Figures 5 and 6 show that the response of the model replicates the major features of the limb motions and ground reaction forces generated during the jump. During the preparatory countermovement phase of the CMJ, the model and our subjects exhibit similar range of motion at the ankle, knee, and hip (Fig. 5 ankle, knee, and hip, compare light and heavy solid lines with shaded regions at 80, 75, and 70 percent of ground contact time, respectively). Peak vertical forces predicted by the optimal control and parameter optimization solutions are approximately 3.5 and 2.5 times body weight respectively (Fig. 6 vertical, light and heavy solid lines), whereas our subjects generated peak forces anywhere between 1.8 and 3.2 times body weight (Fig. 6 vertical, shaded region). In addition, both the model and our subjects generated fore-aft ground reaction forces that were less than 50 percent of body weight (Fig. 6, horizontal).

Minor differences between model and experiment are, however, apparent. Both the optimal control and parameter optimization solutions predict a *steeper* increase in the vertical ground reaction as the body nears its lowest position of the countermovement (Fig. 6 vertical, compare light and heavy solid lines with shaded region at 60–70 percent of ground contact time), as well as a more rapid decrease near lift-off (Fig. 6 vertical, 100 percent of ground contact time). The latter anomaly results from increasing joint angular velocities generated by the model just prior to lift-off, which contradicts the way our subjects actually jumped (joint angular velocities for our subjects *decreased* near lift-off (not shown)).

As yet, we cannot offer any explanation as to why the model predicts a steeper increase in the vertical ground force prior to upward propulsion. We have, however, tested the hypothesis that this difference is due to a one-segment representation of HAT dynamics. In a separate set of experiments, to prevent significant spinal flexure, we constrained the torso by strapping a light, stiff, wooden column longitudinally to each subject's back. With all other conditions unchanged, we found little difference in either the ground reaction forces or limb motions generated during a maximum-height CMJ. We conclude, there-

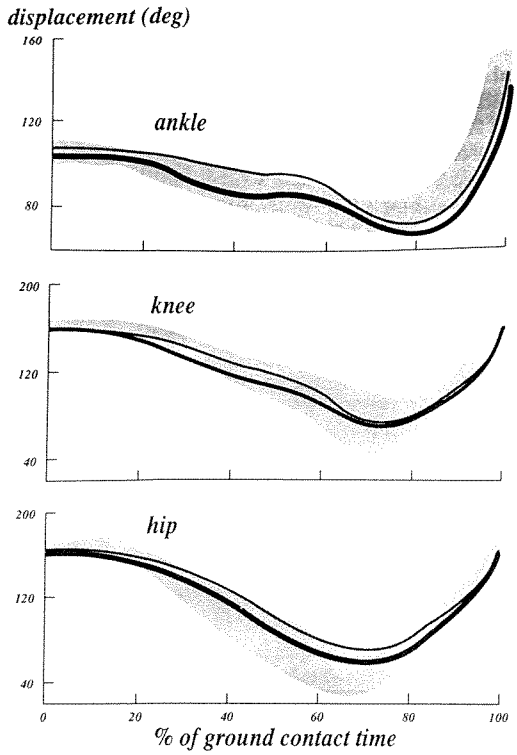

Fig. 5 Parameter optimization algorithm (heavy solid lines), optimal control algorithm (light solid lines), and experimental (shaded regions) joint angular displacements during the ground contact phase of jumping (0 to 100 percent). The experimental trajectories correspond to the range of each subject's highest jump. For each subject, 0 percent of ground contact time defines the instant that the vertical ground force decreases to 95 percent of body weight. 100 percent defines the instant the body leaves the ground for the model and our subjects. For the model, prior to and at 0 percent of ground contact time, muscle forces were computed to maintain the body in static equilibrium. Notice that the parameter optimization algorithm predicts more flexion at the ankle, knee, and hip during the jump. Full extension at each joint is 180 degrees.

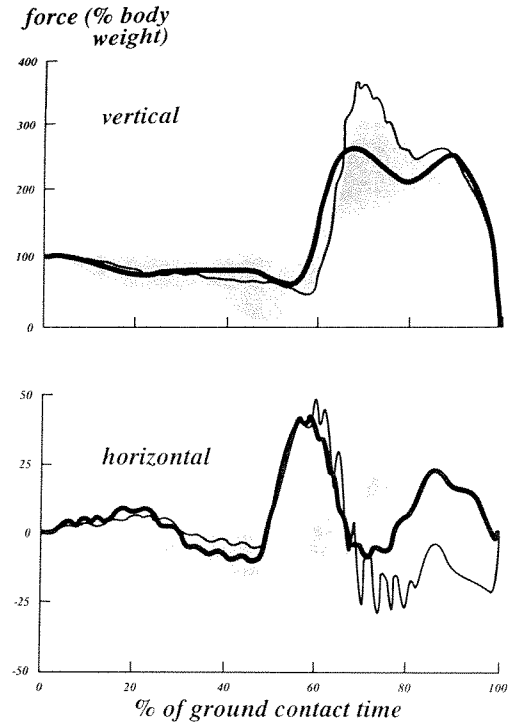

Fig. 6 Parameter optimization algorithm (heavy solid lines), optimal control algorithm (light solid lines), and experimental (shaded regions) vertical and horizontal (fore-aft) ground reaction forces generated during the ground contact phase of jumping (0 to 100 percent). The experimental trajectories correspond to the range of each subject's highest jump. The high frequency ripple in the predicted ground reaction forces (light and heavy solid lines) is an artifact of the torque exerted by the torsional spring placed at the toes to keep the foot flat on the ground prior to heel lift-off.

fore, in agreement with findings by others [29], that a one-segment model for HAT dynamics is adequate. Instead, we hypothesize that the above difference between model and experiment is due to an under-estimation in our model of the rise time (τ_{rise}) for muscle excitation-contraction dynamics (Eqs. (31) and (32)).

Experimental EMG activity was found to agree qualitatively well with the computed optimal controls (compare heavy solid and dashed lines with light wavy lines in Fig. 7). Both the optimal control (heavy dashed lines) and parameter optimization (heavy solid lines) solutions predict a stereotypic proximal-to-distal sequence of muscle activation (i.e., in the order hip, knee, and ankle) for all the uniarticular extensor muscles (see also [29, 30]). Contrary to experiment, however, the model predicts that the uniarticular flexor muscle tibialis anterior is initially activated to produce ankle dorsiflexion during countermovement, while the biarticular rectus femoris is activated early to accelerate the trunk into flexion (Fig. 7 TA and RF, compare heavy solid and dashed lines with light wavy lines). These differences, we believe, are due to an attempt by TA and RF in our model to compensate for the absence of uniarticular knee and hip flexor muscles which act to accelerate the trunk downward during the preparatory, countermovement phase [31].

Optimal and Near-Optimal Controls. Our results tend to support the hypothesis that, at least for the propulsion phase of jumping, the optimal controls are bang-bang [3, 5]. In general, the near-optimal controls predicted by the parameter optimization algorithm closely approximate the bang-bang optimal controls (Fig. 7, 50–100 percent of ground contact time; compare heavy solid and dashed lines), and each of these compare favorably with the pattern of muscle activity recorded during the jump (Fig. 7, 50–100 percent of ground contact time; compare heavy solid and dashed lines with light wavy lines). Specifically, all uniarticular extensor muscles, once activated, remain fully activated until lift-off (e.g., Fig. 7, VAS). Biarticular muscles, on the other hand, do *not* (e.g., Fig. 7, GAS). Consistent with our previous findings for a maximum-height squat jump [30], the latter result suggests that biarticular muscles are concerned more with fine-tuning coordination than with accelerating and delivering power to the individual body segments during the ground contact phase of jumping.

Irrespective of whether the optimal control or parameter optimization algorithm is used, the model is able to reproduce the major features of a maximum-height CMJ. The parameter optimization algorithm, however, yields slightly better agreement with experiment (Fig. 8, compare heavy solid line with shaded region). While the bang-bang optimal controls generate a peak vertical acceleration of the center of mass of the model of 25 m/s^2, the parameter optimization algorithm predicts a value of 15 m/s^2, which compares well with the calculated mean experimental value of 14 m/s^2 (Fig. 8(a), shaded region at 70 percent of ground contact time). Peak vertical displacements and velocities at lift-off, however, are very nearly the same for the optimal control and parameter optimization solutions (Fig. 8(b) and (c), compare light and heavy solid lines at 100 percent of ground contact time), which is consistent with the fact that predicted jump heights differ by only 3 cm (Eq. (33)).

Interestingly, a noticeable difference between the optimal control and parameter optimization solution is that the latter

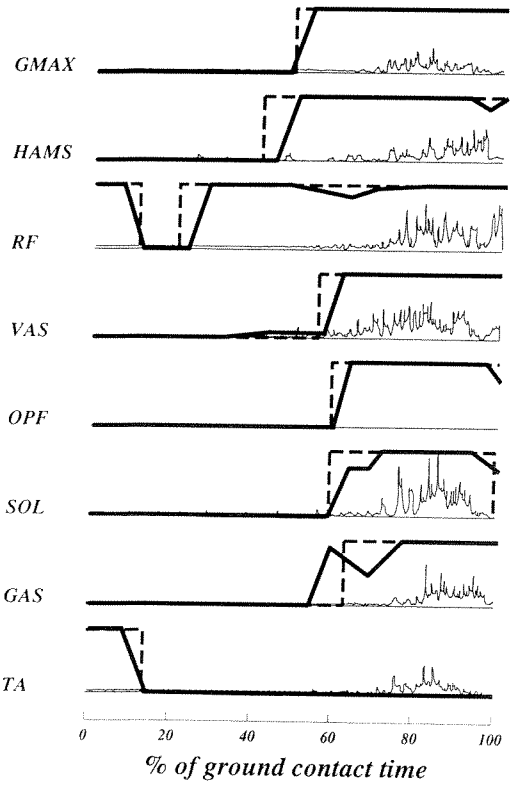

Fig. 7 Rectified experimental EMG activity (light wavy lines) recorded from one subject and the muscle excitation signals ($u(t)$) predicted by the parameter optimization algorithm (heavy solid lines) and optimal control algorithm (heavy dashed lines) during the ground contact phase of jumping. Notice that the sequence of muscle activation is, in general, proximal-to-distal. No EMG activity was recorded from OPF because these are deep lying muscles of the calf.

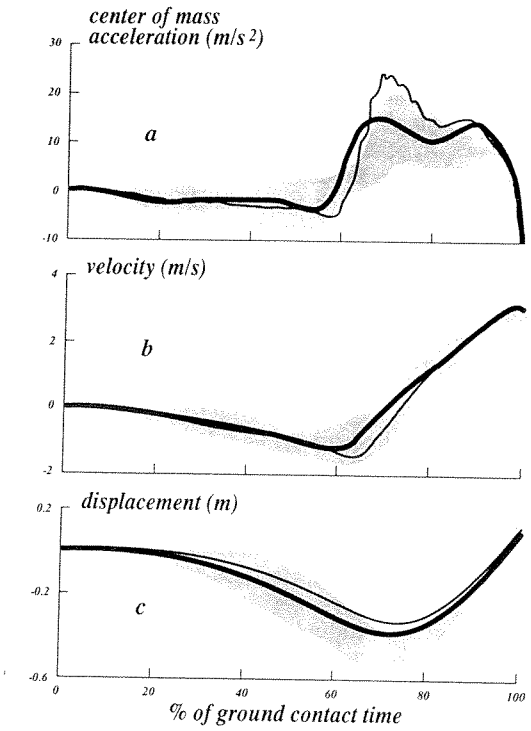

Fig. 8 Parameter optimization algorithm (heavy solid lines), optimal control algorithm (light solid lines), and experimental (shaded regions) vertical acceleration (*a*), vertical velocity (*b*), and vertical displacement (*c*) of the center of mass of the body during the ground contact phase of jumping. Trajectories of the vertical acceleration, vertical velocity, and vertical displacement of the center of mass of each subject during the ground contact phase of jumping were obtained directly from the measured vertical ground reaction force. Specifically, we used the vertical ground reaction to compute the vertical acceleration of the center of mass of the body, and then numerically integrated this trajectory to obtain trajectories of the vertical velocity and vertical displacement of the whole-body center of mass. Zero vertical displacement of the center of mass of the model and our subjects corresponds to standing. Notice that the parameter optimization algorithm predicts more countermovement of the center of mass of the model prior to upward propulsion.

involves significantly more countermovement in the model prior to upward propulsion (Fig. 8(*c*), compare heavy and light solid lines at 70 percent of ground contact time), which agrees more closely with the way our subjects actually jumped (Fig. 8(*c*), compare heavy solid line with shaded region). In agreement with work done by others on cats [32] and humans [3], this result suggests that while the propulsion phase of a maximum-height CMJ may be bang-bang, the preparatory, countermovement phase is probably *not*. That is, our near-optimal, non-bang-bang controls deliver a response of the model that more closely resembles the way our subjects actually countermoved during the preparatory phase of the jump.

Discussion

Though the use of optimal control theory to solve human movement synthesis problems is widely appreciated [33], its full potential has yet to be realized. The reason is that a detailed, dynamical model of the human musculotendinoskeletal system is characterized by severe nonlinearities, heavy coupling, and high dimensionality (i.e., there are many states) (Eqs. (29)–(31)). As a result, optimal control solutions for human movement are hindered by serious computational difficulties. Gradient-based methods [9, 34], for example, must cope with the highly nonlinear characteristics of the costate variables, and, as a result, are plagued by round-off and truncation errors [35]. In contrast, the parameter optimization approach is attractive because it dispenses with the need to solve the TPBVP derived from the necessary conditions of optimal control. Most importantly, and in difference to the modified Polak-Mayne algorithm [28], this method is especially well suited to solving general (i.e., bang-bang as well as non-bang-bang) optimal control problems involving large-scale musculoskeletal systems.

An important feature of both the optimal control and parameter optimization algorithm is that neither guarantee the identification of a global optimum. In fact, as a general rule, the existence of a global optimum can only be verified through the introduction of different initial guesses. We believe that the results derived for jumping using the optimal control and parameter optimization algorithms represent global optima since each algorithm converged to the same solution irrespective of the initial guess. We note here that both algorithms required approximately the same amount of dedicated CPU time (about 48 hr) to converge to a solution on a Silicon Graphics Personal IRIS workstation (4D/25; 16 Mips, 1.6 Mflops).

Whether or not the parameter optimization algorithm converges depends largely upon the accuracy of the first derivatives of the performance index and the constraints (Fig. 1, Step 4). Our experience has been that forward differences yield sufficiently accurate estimates of these quantities to allow the algorithm to proceed to a point where changes in the performance index become negligible. To test the robustness of this result, we have also used central differences to recompute the values of the first derivatives in the parameter optimization problem for jumping. Finding little change in the predicted performance index and controls, we conclude that forward differences are not only acceptable in terms of computational accuracy, but they are in fact preferable due to the considerable

decrease in computational time involved (i.e., central differences require twice as many forward integrations of the system differential equations).

A major advantage of the parameter optimization algorithm is its ability to cope with systems characterized by dynamical discontinuities. In general, differential dynamic programming and gradient-based methods impose strict continuity requirements on algorithms which solve the TPBVP. In fact, such algorithms are usually required to be continuous to, at least, first order. Human movement, however, often involves the presence of dynamical discontinuities. Prior to heel-off during a vertical jump, for example, with the foot constrained to remain flat on the ground, the ground represents a discontinuity in the system differential equations. Specifically, if the model for skeletal dynamics should have four degrees of freedom subsequent to heel-off, it would have only three while the foot remains flat on the ground. Such a change in system dimension imposes discontinuities in the state variables which violate the smoothness requirements of optimal control theory. Fortunately, the parameter optimization approach requires only that the system differential equations be integrated forwards in time to obtain the values of the performance index, the constraints, and their first derivatives. Because this method does not impose any continuity requirements on the state variables or their derivatives, it can be implemented irrespective of whether system dynamics is continuous or not.

We have also tested the robustness of our parameter optimization algorithm by applying it to activities other than vertical jumping. Recently, we formulated and solved a minimum-energy optimal control problem for a sit-to-stand task [36]. Under the assumption that rising from a seated position is characterized by a minimum metabolic energy criterion, we derived an expression for overall metabolic energy expenditure, defined as the sum of muscle activation heat rate, muscle maintenance heat rate, muscle shortening heat rate, muscle mechanical work rate, and the rate of energy dissipation in the passive structures [37, 38]. Using the musculoskeletal model given in Fig. 2, and parameterizing each control history with 21 nodal points, we then computed the non-bang-bang controls for a sit-to-stand maneuver. Comparison of the limb motions, ground reaction forces, and muscle excitations predicted by the model with those generated by five normal subjects performing the same activity [36] has further increased our confidence in the ability of the parameter optimization algorithm to solve general optimal control problems for human movement.

There are, however, computational difficulties surrounding the use of our parameter optimization algorithm, particularly as system dimension becomes very large. For example, when simulating human movement using a three-dimensional musculoskeletal model with many muscles, computation of the first derivatives of the performance index and the constraints with respect to the unknown variables (controls) becomes prohibitive. Since each iteration of the parameter optimization algorithm requires forward integrating the system differential equations at least as many times as there are number of control nodes, performing these integrations consecutively (or serially) is computationally exhaustive, and may even prove unmanageable for very high-dimension systems. An attractive alternative, and one made possible by the emergence of massively parallel machines (e.g., the Intel iPSC/860 Parallel Processor), involves modifying the structure of our algorithm so that the aforementioned computations can be performed in *parallel*. Ideally, each iteration of the parallel-based algorithm will require no more CPU time than that needed to perform a single forward integration of the system differential equations. We are planning to use such an algorithm, in conjunction with a three-dimensional, 14 degree-of-freedom model of the skeleton, actuated by 42 musculotendinous units, to solve an optimal control problem for human walking.

Acknowledgments

We thank Lawrence Abraham, Felix Zajac, and Art Kuo for carefully reviewing an earlier version of this manuscript. We are also indebted to Jim Ziegler for his help with the jumping experiments. This work was supported by the Whitaker Foundation, NASA/Ames Research Center, and St. David's Rehabilitation Center, Austin, Texas.

References

1 Chow, C. K., and Jacobson, D. H., "Studies of Human Locomotion Via Optimal Programming," *Math. Biosci.*, Vol. 10, 1971, pp. 239-306.

2 Hatze, H., "The Complete Optimization of a Human Motion," *Math. Biosci.*, Vol. 28, 1976, pp. 99-135.

3 Levine, W. S., Zajac, F. E., Belzer, M. R., and Zomlefer, M. R., "Ankle Controls that Produce a Maximal Vertical Jump When Other Joints Are Locked," *IEEE Trans. Auto. Contr.*, Vol. AC-28 (11), 1983, pp. 1008-1016.

4 Davy, D. T., and Audu, M. L., "A Dynamic Optimization Technique for Predicting Muscle Forces in the Swing Phase of Gait," *J. Biomech.*, Vol. 20, 1987, pp. 187-201.

5 Pandy, M. G., Zajac, F. E., Sim, E., and Levine, W. S., "An Optimal Control Model for Maximum-Height Human Jumping," *J. Biomech.*, Vol. 23, 1990, pp. 1185-1198.

6 Crowninshield, R. D., "Use of Optimization Techniques to Predict Muscle Forces," ASME JOURNAL OF BIOMECHANICAL ENGINEERING, Vol. 100, 1978, pp. 88-92.

7 Hardt, D. E., "Determining Muscle Forces in the Leg During Human Walking: An Application and Evaluation of Optimization Methods," ASME JOURNAL OF BIOMECHANICAL ENGINEERING, Vol. 100, 1978, pp. 72-78.

8 Kirk, D. E., *Optimal Control Theory: An Introduction*, Prentice-Hall, Englewood Cliffs, NJ, Chapter 4, 1970.

9 Bryson, A. E., and Ho, Y. C., *Applied Optimal Control*, Hemisphere, Washington, Chapter 7, 1975.

10 Sirisena, H. R., and Tan, K. S., "Computation of Constrained Optimal Controls Using Parameterization Techniques," *IEEE Trans. Auto. Contr.*, Vol. AC-19, 1974, pp. 431-433.

11 Nagurka, M. L., and Yen, V., "Fourier-Based Optimal Control of Nonlinear Dynamic Systems," ASME *Journal of Dynamic Systems, Measurement and Control*, Vol. 112, 1990, pp. 17-26.

12 Goh, C. J., and Teo, K. L., "Control Parameterization: A Unified Approach to Optimal Control Problems with General Constraints," *Automatica*, Vol. 24, 1988, pp. 3-18.

13 Nguyen, H. N., "Optimal Solutions to Flight Mechanics Problems Using a Nonlinear Programming and Collocation Technique," *Proc. of AIAA Guidance, Navigation, and Control Conference*, Portland, Oregon, 1990, pp. 911-922.

14 Hodges, D. H., and Bless, R. R., "Weak Hamiltonian Finite Element Method for Optimal Control Problems," *J. Guidance, Control, and Dynamics*, Vol. 14, 1991, pp. 148-156.

15 Powell, M. J. D., "A Fast Algorithm for Nonlinearly Constrained Optimization Calculations," Matson, G. A. (ed), *Numerical Analysis: Lecture Notes in Mathematics*, Springer-Verlag, Vol. 630, 1978, pp. 144-157.

16 Zajac, F. E., "Muscle and Tendon: Properties, Models, Scaling, and Application to Biomechanics and Motor Control," *CRC Critical Rev. Biomed. Engng.*, ed., Bourne, J. R., Vol. 17, 1989, pp. 359-411. CRC Press, Boca Raton.

17 He, J., "A Feedback Control Analysis of the Neuro-Muscular-Skeletal System of a Cat Hindlimb," Ph.D. thesis, Electrical Engineering Department, University of Maryland, College Park, MD, 1988.

18 Wickiewicz, T. L., Roy, R. R., Powell, P. L., and Edgerton, V. R., "Muscle Architecture of the Human Lower Limb," *Clin. Orthop. Rel. Res.*, Vol. 179, 1983, pp. 275-283.

19 Brand, R. A., Pedersen, D. R., and Friederich, J. A., "The Sensitivity of Muscle Force Predictions to Changes in Physiological Cross-Sectional Area," *J. Biomech.*, Vol. 19, 1986, pp. 589-596.

20 Alexander, R.McN., and Vernon, A., "The Dimensions of Knee and Ankle Muscles and the Forces They Exert," *J. Hum. Mvmt. Stud.*, Vol. 1, 1975, pp. 115-123.

21 Woo, S., Gomez, M. A., Woo, Y., and Akeson, W. H., "Mechanical Properties of Tendons and Ligaments. II. The Relationships of Immobilization and Exercise on Tissue Remodeling," *Biorheology*, Vol. 19, 1982, pp. 397-408.

22 Butler, D. L., Grood, E. S., Noyes, F. R., Zernicke, R. F., and Brackett, K., "Effects of Structure and Strain Measurement Technique on the Material Properties of Young Human Tendons and Fascia," *J. Biomech.*, Vol. 17, 1984, pp. 239-306.

23 Winter, D. A., *Biomechanics of Human Movement*, Wiley, New York, 1979, pp. 150-152.

24 Brand, R. A., Crowninshield, R. D., Wittstock, C. E., Pedersen, D. R., Clark, C. R., and van Krieken, F. M., "A Model for Lower Extremity Muscular Anatomy," ASME JOURNAL OF BIOMECHANICAL ENGINEERING, Vol. 104, 1982, pp. 304-310.

25 Smidt, G. L., "Biomechanical Analysis of Knee Flexion and Extension," *J. Biomech.*, Vol. 6, 1973, pp. 79-92.

26 Pandy, M. G., and Zajac, F. E., "Dependence of Jumping Performance on Muscle Strength, Muscle-Fiber Speed, and Tendon Compliance," Stein, J. L. Ashton-Miller, J. A., and Pandy, M. G., eds. *Issues in the Modeling and*

Control of Biomechanical Systems, ASME, New York, Vol. DSC-17, 1989, pp. 59-63.

27 Polak, E., and Mayne, D. Q., "First-order Strong Variation Algorithms for Optimal Control," *J. Opt. Theory and Appl.*, Vol. 16, No. 3, 1975, pp. 277-301.

28 Sim, E., "The Application of Optimal Control Theory for Analysis of Human Jumping and Pedaling," Ph.D. Thesis, Department of Electrical Engineering, University of Maryland, College Park, MD, 1988.

29 Bobbert, M. F., and van Ingen Schenau, G., "Coordination in Vertical Jumping," *J. Biomech.*, Vol. 21, 1988, pp. 249-262.

30 Pandy, M. G., and Zajac, F. E., "Optimal Muscular Coordination Strategies for Jumping," *J. Biomech.*, Vol. 24, 1991, pp. 1-10.

31 Anderson, F. C., and Pandy, M. G., 1991, Unpublished results.

32 Zajac, F. E., "Thigh Muscle Activity During Maximum-Height Jumps by Cats," *J. Neurophysiology*, Vol. 53, No. 4, 1985, pp. 979-994.

33 Hatze, H., "Neuromusculoskeletal Control Systems Modelling—A Critical Survey of Recent Developments," *IEEE Trans. Auto. Contr.*, Vol. AC-25, 1980, pp. 375-385.

34 Miele, A., "Recent Advances in Gradient Algorithms for Optimal Control Problems," *J. Opt. Theory and Appl.*, Vol. 17, 1980, pp. 1-52.

35 Pandy, M. G., Zajac, F. E., Hoy, M. G., Topp, E., Tashman, S., Stevenson, P. J., Cady, C. T., Sim, E. and Levine, W. S., "Sub-optimal Control of a Maximum-height, Countermovement Jump," Stein, J. L. (ed.): *Modeling and Control Issues in Biomechanical Systems*, ASME, New York, Vol. DSC-12: 1988, pp. 27-44.

36 Heekin, A. M., Garner, B. A., and Pandy, M. G., "Optimal Control Solutions for Standing Up: Formulation and Evaluation of Performance Criteria," Vanderby, R., ed., *1991 Advances in Bioengineering*, ASME, New York, Vol. BED-20: pp. 513-516.

37 Hatze, H., and Buys, J. D., "Energy-Optimal Controls in the Mammalian Neuro-Muscular System," *Biol. Cybern.*, Vol. 27, 1977, pp. 9-20.

38 Khang, G., and Zajac, F. E., "Paraplegic Standing Controlled by Functional Neuro-Muscular Stimulation: Part I—Computer Model and Control-System Design," *IEEE Transactions on Biomedical Engineering*, Vol. 36 (9), 1989, pp. 873-884.

39 Leondes, C. T., and Wu, C. A., "Initial Condition Sensitivity Functions and Their Applications," ASME *Journal of Dynamic Systems, Measurement and Control*, Vol. 5, 1971, pp. 116-122.

40 Hoy, M. G., Zajac, F. E., and Gordon, M. E., "A Musculoskeletal Model of the Human Lower Extremity: The Effect of Muscle, Tendon, and Moment Arm on the Moment-Angle Relationship of Musculotendon Actuators at the Hip, Knee, and Ankle," *J. Biomech.*, Vol. 23, 1990, pp. 157-169.

41 Inman, V. T., Ralston, H. J., and Todd, F., *Human Walking*, Williams and Wilkins, Baltimore, Chapter 4, 1981.

42 Sale, D., Quinlan, J., Marsh, E., McComas, A. J., and Belanger, A. Y., "Influence of Joint Position on Ankle Plantarflexion in Humans," *J. Appl. Physiol.: Respirat., Environ. Exer. Physiol.*, Vol. 52, 1982, pp. 1636-1642.

43 Lindahl, O., Movin, A., and Rindquist, I., "Knee Extension Measurement of the Isometric Force in Different Positions of the Knee Joint," *Acta Orthop. Scand.*, Vol. 40, 1969, pp. 79-85.

44 Nemeth, G., Ekholm, J., Arborelius, U., Harms-Ringdahl, K., and Schuldt, K., "Influence of Knee Flexion on Isometric Hip Extensor Strength," *Scand. J. Rehab. Med.*, Vol. 15, 1983, pp. 97-101.

45 Waters, R. L., Perry, J., McDaniels, J. M., and House, K., "The Relative Strength of the Hamstrings During Hip Extension," *J. Bone Jt. Surg.*, Vol. 56-A, 1974, pp. 1592-1597.

APPENDIX

To demonstrate the validity of the parameter optimization approach, we present here the solution to a standard optimal control problem. This example, borrowed from Leondes and Wu [39], involves a nonlinear functional, linear system differential equations, control-variable inequality constraints, and a fixed final time. The optimal control problem is to minimize

$$J=\frac{1}{2}\int_0^5 (x_1^2+x_2^2)dt \tag{A-1}$$

subject to the system differential equations

$$\dot{x}_1=x_2$$
$$\dot{x}_2=x_2-x_1+u, \tag{A-2}$$

the boundary conditions

$$x_1(0)=0.231$$
$$x_2(0)=1.126, \tag{A-3}$$

and the control-inequality constraints

$$-0.8\le u\le 0.8. \tag{A-4}$$

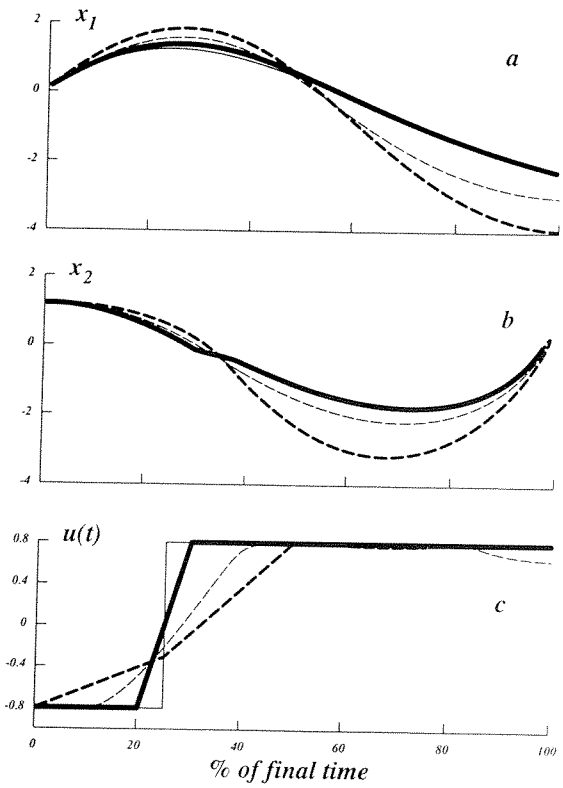

Fig. A-1 State trajectories (*a*)-(*b*) and control history (*c*) predicted by the parameter optimization algorithm using 5 and 21 control nodes (heavy dashed and solid lines, respectively), the theoretical bang-bang solution reported by Leondes and Wu [39] (light solid lines), and the Fourier-based method described by Nagurka and Yen [11] (light dashed lines). The parameter optimization solution with 21 nodes approximates the theoretical bang-bang optimal controls much more closely than the corresponding solution with only 5 control nodes. Note that the heavy and light solid lines in (*a*) and (*b*) are almost indistinguishable. Note also that the near-optimal controls and state trajectories predicted by the parameter optimization algorithm using 21 control nodes (heavy solid lines) are more accurate than the solution derived using the Fourier-based method (light dashed lines).

Introducing the transformation given in Eq. (21) to normalize time, the system differential equations (Eq. (A-2)) become

$$x_1'=t_f x_2$$
$$x_2'=t_f(x_2-x_1+u);\quad 0\le\tau\le 1;\quad x_i'=\frac{dx_i}{d\tau}\ (i=1,2) \tag{A-5}$$

where t_f is the final time ($t_f=5$ s; Eq. (A-1)). A computational solution to this problem was found by parameterizing the control history ($u(t)$) using both 5 and 21 nodal points. The near-optimal controls and states predicted by the parameter optimization algorithm are shown in Fig. A-1 (heavy dashed and solid lines). Also given is the optimal control solution derived from a solution of the TPBVP [39] (light solid lines), as well as the near-optimal solution computed by Nagurka and Yen [11] using the Fourier-based method (light dashed lines). The optimal controls are bang-bang (Fig. A-1 (*c*), light solid lines), and the optimal performance index (Eq. (A-1)) is $J^*=5.86$ [39].

With only 5 nodal points, the parameter optimization algorithm *cannot* approximate the optimal control solution accurately (Fig. A-1, compare heavy dashed with light (or heavy) solid lines). In fact, the predicted optimal performance is 16.99, which differs by almost 200 percent from the value derived by solving the TPBVP [39]. The reason is that, with only 5 nodal points representing the control history, the accuracy with which the optimal switching time can be estimated is rather crude

(i.e., 5 nodal points produce a grid size of only 0.25 t_f s). As a result, the parameter optimization algorithm cannot converge to the theoretical, instantaneous result.

Increasing the number of nodal points to 21 yields a much better approximation to the bang-bang solution. The predicted optimal performance index is now 5.97, which is only 1.9 percent larger than the value generated by the bang-bang optimal control. With the nodal-point spacing now at 0.05 t_f s, the parameter optimization algorithm is able to change the control history ($u(t)$) more quickly, and therefore approximate the instantaneous switching time more accurately (Fig. A-1(c)), compare light and heavy solid lines). Clearly, in the limit, an infinite number of nodal points are needed to replicate the bang-bang optimal control. Nevertheless, the parameter optimization algorithm, with 21 control nodes, is able to produce state trajectories that are nearly identical with those generated by the bang-bang optimal control (Fig. A-1(a)-(b), light and heavy solid lines are almost indistinguishable).

Figure A-1 also shows that, in this case, the parameter optimization algorithm is superior to the Fourier-based method proposed by Nagurka and Yen [11] (compare heavy solid lines with light dashed lines). Even with a 4-term series approximation for the state variables, the Fourier-based optimal control can only change its value in 0.4 t_f s, which results in the predicted state trajectories being noticeably different from those computed using the bang-bang control (Fig. A-1(a)-(b), compare light (or heavy) solid lines with light dashed lines). In fact, as noted by Nagurka and Yen [11], the Fourier-based method is, in general, unsuitable for computing optimal controls that are bang-bang.